Journal of Inorganic Biochemistry 220 (2021) 111455

Contents lists available at ScienceDirect

Journal of Inorganic Biochemistry

journal homepage: www.elsevier.com/locate/jinorgbio

Distal lysine (de)coordination in the algal hemoglobin THB1: A combined computer simulation and experimental study

Laia Julió Plana [a], Jaime E. Martinez Grundman [b], Darío A. Estrin [a], Juliette T.J. Lecomte [b,*], Luciana Capece [a,**]

[a] Departamento de Química Inorgánica, Analítica y Química Física/INQUIMAE-CONICET, Facultad de Ciencias Exactas y Naturales, Universidad de Buenos Aires, Buenos Aires, Argentina
[b] T. C. Jenkins Department of Biophysics, Johns Hopkins University, Baltimore, MD 21218, United States

ARTICLE INFO

Keywords:
THB1
Molecular dynamics
Truncated hemoglobins
Hexacoordination
Lysine ionization
QM/MM calculation

ABSTRACT

THB1 is a monomeric truncated hemoglobin from the green alga *Chlamydomonas reinhardtii*. In the absence of exogenous ligands and at neutral pH, the heme group of THB1 is coordinated by two protein residues, Lys53 and His77. THB1 is thought to function as a nitric oxide dioxygenase, and the distal binding of O_2 requires the cleavage of the Fe–Lys53 bond accompanied by protonation and expulsion of the lysine from the heme cavity into the solvent. Nuclear magnetic resonance spectroscopy and crystallographic data have provided dynamic and structural insights of the process, but the details of the mechanism have not been fully elucidated. We applied a combination of computer simulations and site-directed mutagenesis experiments to shed light on this issue. Molecular dynamics simulations and hybrid quantum mechanics/molecular mechanics restrained optimizations were performed to explore the nature of the transition between the decoordinated and lysine-bound states of the ferrous heme in THB1. Lys49 and Arg52, which form ionic interactions with the heme propionates in the X-ray structure of lysine-bound THB1, were observed to assist in maintaining Lys53 inside the protein cavity and play a key role in the transition. Lys49Ala, Arg52Ala and Lys49Ala/Arg52Ala THB1 variants were prepared, and the consequences of the replacements on the Lys (de)coordination equilibrium were characterized experimentally for comparison with computational prediction. The results reinforced the dynamic role of protein–propionate interactions and strongly suggested that cleavage of the Fe–Lys53 bond and ensuing conformational rearrangement is facilitated by protonation of the amino group inside the distal cavity.

1. Introduction

Truncated hemoglobins (TrHbs) are widely distributed in unicellular organisms and plants. These proteins constitute a distinct lineage of the hemoglobin (Hb) superfamily [1–5], differing from the canonical globins (e.g., myoglobin, Mb) in that they typically contain ~30 fewer amino acid residues. This difference in the length of the polypeptide chain is accompanied by a change in the three-dimensional structure. For example, while Mb displays a 3-over-3 helical sandwich fold, TrHbs display a smaller 2-over-2 fold [6] (Fig. 1A). Even though TrHbs have been the subject of many experimental and computational studies in the last several years [7–16], the physiological functions of most TrHbs remain to be elucidated. Detailed mechanistic and structural studies, however, are particularly useful in characterizing the range of plausible physicochemical properties TrHbs can exhibit in comparison to well-studied 3-over-3 Hbs.

THB1 is a cytoplasmic TrHb from the chlorophyte *Chlamydomonas reinhardtii* [17]. The current hypothesis regarding THB1 function is related to the modulation of nitrate, nitrite, and nitric oxide concentrations through its nitric oxide dioxygenase (NOD) activity [18–20]. This activity appears to be THB1's chief function and involves the conversion of O_2 and NO to NO_3^-. Under physiological conditions, THB1 contains a type *b* heme coordinated with His77 (F8 in the Mb nomenclature) on the proximal side and Lys53 (E10) on the distal side [18], in an endogenous hexacoordinate (6c, His–Fe–Lys) scheme.

The dioxygenation reaction requires the cleavage of the Fe–Lys53

* Corresponding author at: T.C. Jenkins Department of Biophysics, Johns Hopkins University, 3400 North Charles Street, Baltimore, MD 21218, United States.
** Corresponding author at: Dto. de Química Inorgánica, Analítica y Química Física - INQUIMAE-CONICET, Fac. de Ciencias Exactas Y Naturales, Univ. de Buenos Aires, Cdad. Universitaria, CABA C1428EGA, Argentina.
E-mail addresses: lecomte_jtj@jhu.edu (J.T.J. Lecomte), lula@qi.fcen.uba.ar (L. Capece).

https://doi.org/10.1016/j.jinorgbio.2021.111455
Received 13 October 2020; Received in revised form 26 March 2021; Accepted 27 March 2021
Available online 5 April 2021
0162-0134/© 2021 Elsevier Inc. All rights reserved.

coordination bond so that an O_2 molecule can bind on the distal side and react with the second substrate, NO (Scheme 1). The reaction mechanism starting from the pentacoordinate (5c, deoxy) state has been studied in several members of the Hb superfamily [12,21–23]. However, a growing number of Hbs from all lineages similarly require the release of an endogenous ligand to allow coordination of an exogenous ligand, be it O_2 or some other molecule [24]. THB1 is particularly convenient for the study of such 6c ⇄ 5c transition, while also showcasing Fe–Lys coordination, a property that lacks extensive experimental and theoretical work compared to other well-known 6c states (e.g., His–Fe–His and His–Fe–Met).

Inspection of the available THB1 X-ray structures (Protein Data Bank (PDB) IDs 4XDI and 6CII) indicates that decoordination of Lys53 and replacement with an exogenous ligand (such as cyanide in the Fe(III) state) lead to a new conformation of the distal heme pocket. This conformational change involves the movement of Lys53 from the heme cavity to the protein–solvent interface (Fig. 1B) and a simultaneous introduction of polar, hydrogen-bonding residues (Tyr29, Gln50, and Gln54) favoring the stabilization of negative charge density on the bound O_2, which is crucial for NOD activity [19]. In this work, we refer to these two general conformations as either "in" when Lys53 is inside the heme cavity or "out" when it is outside (5c-out; also "Lys-off" in [25]). Mechanistically and in theory, the "in" conformation could also exist in three states, one with His–Fe–Lys coordination (6c or "Lys-on") and two others with Lys decoordinated (5c-in), either in the neutral or in the protonated state.

Nuclear magnetic resonance (NMR) spectroscopy measurements at equilibrium have provided clues as to the dynamics of the Lys53 side chain. The transition between the 6c state and the 5c-out protonated state is slow on the chemical shift time scale at pH 6.1. Under these conditions, the apparent rate constant for the overall process determined by N_{ZZ} exchange applied to the Fe(II) protein is 25 ± 6.0 s^{-1} in the forward (6c → 5c-out) direction and 7.6 ± 2.0 s^{-1} in the reverse direction (5c-out → 6c) [26]. The point at which protonation of Lys53 occurs in this transition could not be determined from the experimental data, because the 5c-in states described above are not well-populated nor easily identifiable. On the other hand, under conditions of high pH where the 6c state is fully populated [18], NMR experiments show that the process of spontaneous decoordination/recoordination of Lys53 can occur in the μs-ms timescale [26]. Lineshape analysis indicates rate constants of 3500 s^{-1} in the forward direction and ≥ 70,000 s^{-1} in the reverse direction at pH 9.6. When mixtures of H_2O and D_2O are used as

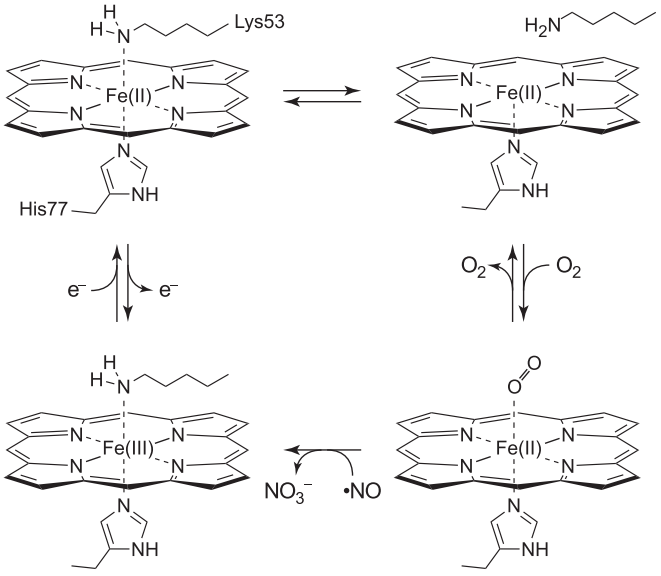

Scheme 1. 6c ⇄ 5c equilibrium and NOD reaction in THB1. In order to bind O_2, the Fe–Lys53 coordination bond must break, allowing THB1 to adopt the 5c state. At some point during the Fe–Lys53 bond cleavage and the exposure of Lys53 to the protein exterior, Lys53 becomes protonated. Reaction of O_2 with NO causes oxidation of the Fe(II) heme to the Fe(III) state. Once the product (NO_3^-) is released, Lys53 is able to coordinate Fe(III) and the enzymatic cycle is completed by reduction to the initial Fe(II) state [18,26].

the solvent, an NHD/NH_2 isotope shift is detected along with slow exchange between NHD and NH_2 isotopologues. These observations support a rapid on-off equilibrium without protonation of the amino group, which generates a briefly decoordinated and neutral Lys53 (5c-in). This 5c-in species can then proceed to the 5c-out and protonated state. Furthermore, in two-dimensional nuclear Overhauser effect spectra collected at pH 9.5, the detection of signals connecting Lys53 NH_2 at its coordinated chemical shifts (−8 ppm) and bulk water (4.7 ppm) is consistent with solvent penetration into the distal cavity. Information at a physiologically relevant pH, however, is not as readily available.

In this work, our aim was to elucidate the mechanism of lysine decoordination and the "in" → "out" conformational transition in THB1 as biochemical prerequisites for NOD activity. In particular, we describe

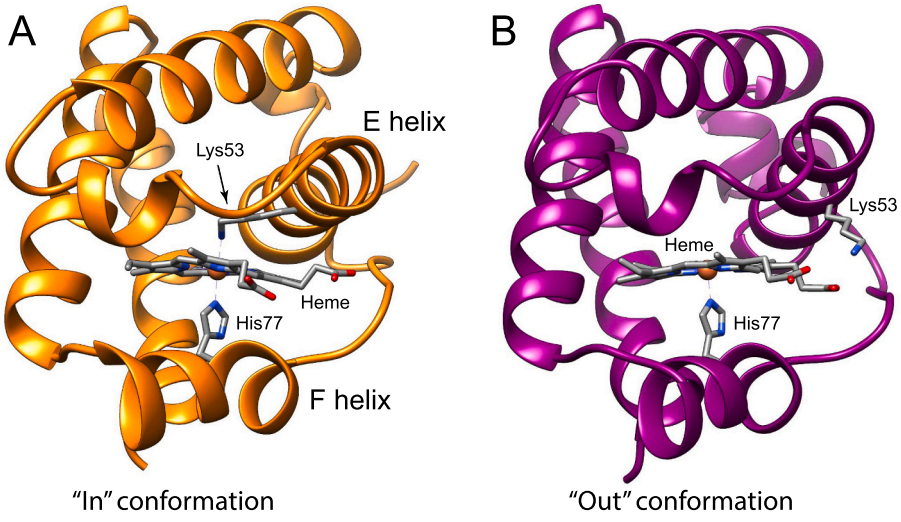

Fig. 1. Available crystal structures of THB1 representing the two main conformational states discussed in this work: A) the hexacoordinate (6c, "in") conformation (PDB ID 4XDI [27]) with proximal His77 and distal Lys53 ligands, and B) the pentacoordinate (5c, "out") conformation generated by removing the distal cyanide ligand from PDB ID 6CII [25]. In this model, Lys53 points toward the protein–solvent interface and interacts with the heme 7-propionate.

the interactions that vary along the transition and the role of Lys53 protonation in the process. We observed that electrostatic interactions involving neighboring Lys49 (E6) and Arg52 (E9) with the heme propionates are involved in the conformational transition, energetically blocking the egress of Lys53 from the distal cavity. Additionally, the results indicate the importance of distal cavity solvation and consequent Lys53 protonation inside the distal cavity to favor the decoordination or lysine expulsion process. Altogether, the results from this work provide an improved description of this particular member of the TrHb family, as well as novel insights into iron coordination and globin conformational energetics in general.

2. Material and methods

2.1. Computational methods

2.1.1. Initial structures

The initial 6c structure of THB1 was obtained from its His–Fe–Lys coordinated X-ray structure (PDB ID 4XDI [27]) in the Fe(III) state. The 5c-in structure was obtained starting from the 6c structure by releasing the Fe–Nζ(Lys53) bond constraint, followed by a minimization and slow equilibration (described below).

2.1.2. Classical molecular dynamic simulations

The classical simulations were performed by using the PMEMD module of the Amber16 package [28]. The starting structures were immersed in an octahedral box of TIP3P water molecules. The minimum distance from the protein surface to the end of the box was 15 Å. Protonation states of ionizable residues were set to correspond to those at neutral pH. As in previous works [7,29–31], the tautomeric state of neutral histidines was established in order to favor H-bond formation. His77 (the "proximal" histidine) coordinates the heme iron with Nε2 and was protonated at Nδ1. The protonation state of the amino group of Lys53 differed depending on the simulation, as explained below. SHAKE was used to keep bonds involving hydrogen atoms at their equilibrium lengths [32], which allowed a time step of 2 fs to be employed for the integration of Newton's equations. All simulations were performed with 1 atm and 300 K conditions and were maintained with the Langevin thermostat [33] (with a collision frequency of 2.0 ps^{-1}) and Berendsen barostat [34] (with a pressure relaxation of 1.0 ps). Equilibration consisted of an energy minimization of the initial structures, followed by a slow heating up to 300 K. We performed 300 ns of MD simulations for wild-type (WT) THB1, as well as for the K49A, R52A, and K49A/R52A variants, which were generated in silico by replacing Lys49 and Arg52 with an Ala residue. The WT systems were simulated in two different Fe (II) heme coordination states: 6c (with Lys53 in the neutral state) and 5c with either neutral Lys53 (5c-Lys) or with protonated Lys53 (5c-LysH^+). For all mutants, only the two 5c heme states were considered. In order to simulate the WT THB1 in the 6c state, the charges for both the heme moiety and the coordinated Lys53 were determined using the Antechamber program of the Amber16 Package. This consists of a RESP charges calculation [35], starting from the electrostatic potential calculated with Gaussian09 [36] using the density functional theory (DFT) B3LYP/6-31G(d,p) (see Supplementary Material for details). For the heme in the 5c state, the parameters corresponded to those developed [37] and used in several heme–protein studies [35,38–43]. Longer simulations (3 μs) were performed for the WT protein in the two 5c-in states: 5c-Lys and 5c-LysH^+. Analysis of the molecular dynamics (MD) simulations was performed using Visual Molecular Dynamics (VMD) [44] and the Cpptraj tool from Amber16 package [28].

2.1.3. Hybrid quantum mechanics-molecular mechanics (QM/MM) calculations

Hybrid QM/MM geometry optimizations were performed with a conjugate gradient algorithm at the DFT level with the SIESTA code with a QM/MM implementation [45,46]. DFT methods, including the SIESTA code, have been shown to describe medium and large systems well and have also proven to be appropriate for biomolecules and, specifically, for heme models [31,47,48]. The QM subsystems were treated at the DFT level as described above, using the PBE exchange correlation functional [49] with a DZVP basis set [50], whereas the classical subsystems were treated using the Amber14 force field parameterization [51]. Schemes of the QM region can be found in the Supplementary Material (Fig. S1). Only residues located within 10 Å of the QM/MM frontier were allowed to move freely. The frontier between the QM and MM portions of the system was treated with the scaled position link atom method [52]. The rest of the protein and the water molecules were treated classically. A similar approach has been applied previously in several heme proteins [37]. Initial structures for the QM/MM calculations were taken from the classical MD simulations, which were cooled down to 0 K before QM/MM calculations. In our system a restriction was applied, as explained below.

Owing to the extensive sampling required for obtaining free energy profiles and the associated computational cost, we opted for potential energy surface calculation, using restrained energy optimizations along a reaction coordinate. In order to perform a potential energy profile, an additional term, $V(\xi) = k(\xi - \xi_0)^2$, was included in the potential energy. The force constant k was set to 200 kcal/mol·$Å^2$, and ξ_0 is a reference value left to vary throughout the reaction coordinate with an interval of 0.05 Å. With this approach, the system is forced to follow the energy minimum reaction path along the given reaction coordinate. A similar approach was applied in previous works to study chemical reactions in heme proteins [53–55].

2.2. Experimental methods

2.2.1. Protein purification

The K49A, R52A and K49A/R52A (or AA) mutations were introduced into the WT THB1 codon-optimized gene on a pJExpress414 plasmid (ATUM, Newark, CA) by PCR using PfuTurbo DNA polymerase (Agilent) and custom primers purchased from Integrated DNA Technologies, Inc. (Coralville, IA). Sequences were verified by GENEWIZ, Inc. (South Plainfield, NJ). The genes were overexpressed in *Escherichia coli* BL21(DE3) cells as previously described [18]. K49A and R52A THB1s accumulated in inclusions bodies. These proteins were purified by urea denaturation and size exclusion chromatography, followed by the addition of porcine hemin chloride (Sigma, 20 mg/ml in 0.1 M NaOH) until full reconstitution was observed by electronic absorption spectroscopy. Anion exchange chromatography removed excess hemin. AA THB1 partitioned primarily in the soluble fraction and in the apoprotein state. This protein was first reconstituted with hemin, then subjected to ion exchange and size exclusion chromatography. Purity was evaluated by sodium dodecyl sulfate polyacrylamide gel electrophoresis and mass spectrometry.

2.2.2. pH titrations of Fe(III) and Fe(II) THB1 variants

The titrations were monitored by electronic absorption spectroscopy with a Varian Cary 50 spectrophotometer and analyzed by singular value decomposition (SVD) and global fitting to determine apparent pK_a and Hill coefficients as described previously [25]. In summary, pH titrations of Fe(III) THB1 variants were carried out with a sample (~3–10 μM on a heme basis) in 5 mM phosphate buffer (pH ~7). This initial sample was split into two samples, one for the acidic range (from pH 7.2 to 4.0) using aliquots of 0.1 M HCl, and the other for the basic range (from pH 7.2 to 12.0) using aliquots of 0.1 M NaOH. Spectra were recorded from 250 to 750 nm in 0.5 nm steps using a 0.25-s averaging time.

pH titrations of Fe(II) THB1 variants were performed with separate samples each containing ~5 μM of Fe(III) protein in 100 mM buffer covering a range of pH from 5.7 to 11.0. Different buffers were used depending on the desired pH (2-(N-morpholino)ethanesulfonic acid for pH 5.7–6.4, 3-(N-morpholino)propanesulfonic acid for pH 6.5–7.5, tris

(hydroxymethyl)aminomethane for pH 7.7–8.4, borate for pH 8.7–9.8, and N-cyclohexyl-3-aminopropanesulfonic acid for 10.1–11.1). Prior to reduction, the spectrum of the Fe(III) state of each sample was collected to determine the concentration of the protein. The Fe(II) state was obtained by adding 2 mM sodium dithionite to the sample and monitoring the reduction as a function of time.

3. Results

In prior work, the pH-dependent 6c ⇄ 5c-out equilibrium and the NOD reaction of THB1 were characterized with various biochemical, structural and spectroscopic strategies [18,26]. Because of the limited mechanistic information obtained from these experiments, several molecular aspects of the transition require further inspection. Specifically, the conspicuous interactions of Lys49 and Arg52 with the heme propionates point to a role in controlling heme coordination [25]. In addition, the influence of Lys53 protonation in driving bond breakage or conformational rearrangement, or both, has not been determined. The results below attempt to shed light on these matters. First, we survey the structural and dynamical basis for the expulsion of Lys53 from the heme cavity by means of classical MD simulations. We then study the Fe–Lys bond cleavage mechanism using QM/MM calculations. Finally, we compare the simulated results with equilibrium characterization of THB1 Ala variants targeting ionic interactions with the heme propionates.

3.1. MD simulations of the in → out transition

3.1.1. WT THB1 simulations

To obtain information on the molecular mechanism of the in → out transition, 300 ns of classical MD simulations were performed with wild-type THB1 starting from the 6c and the 5c-in states. In the 6c state, Lys53 is bound to the iron in the neutral state. In the 5c state, as previously explained, two MD simulations were performed: one with the amino group of Lys53 modelled in the neutral state (WT-Lys) and another with Lys53 modelled in the protonated state (WT-LysH$^+$), as expected when exposed to solvent.

In all cases, the proteins remained globally stable along the time scale of the simulation as monitored by the root-mean-square deviation (RMSD) along the simulation using the original X-ray structure as reference (Fig. S2). The root-mean-square fluctuations (RMSF) along the MD trajectories were also analyzed (Fig. S3) and revealed a significant increase in the CD region (residues 35 to 45) and at the beginning of the E helix (residues 46 to 51) of WT-LysH$^+$ when compared to WT-Lys. In contrast, fluctuations are tempered in the EF loop (residues 64 to 71) when Lys53 is protonated.

Visual inspection of the MD trajectories from the 5c state shows that for WT-LysH$^+$, the 5c-in → 5c-out transition happens spontaneously on the time scale of the MD simulation. For WT-Lys, however, the side chain does not exit the cavity and stays in the 5c-in conformation during the entire simulation. Furthermore, we observed that the basic residues Lys49 and Arg52 interact with the heme propionates (Table S2 shows the percentage of time where Lys49 and Arg52 interact with heme propionates while Lys53 is in the 5c-in conformation), potentially

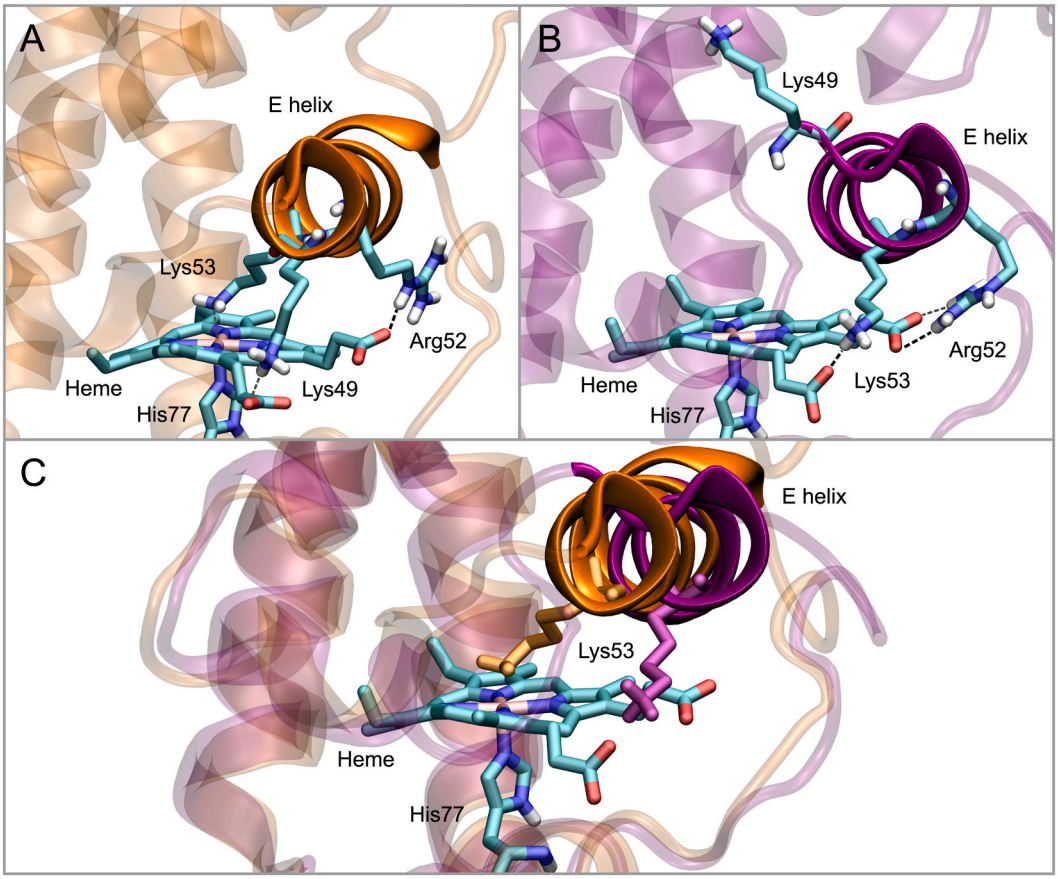

Fig. 2. Typical snapshots during the WT THB1 MD simulations in A) the 5c-in conformation, with neutral Lys53 decoordinated and Lys49 and Arg52 engaging in ionic interactions with heme propionates, and B) the 5c-out conformation, with Lys53 outside the heme cavity and interacting with heme 6-propionate. C) Superimposed 5c-in (orange) and 5c-out structures (purple), highlighting the change in the E helix position. (For interpretation of the references to colour in this figure legend, the reader is referred to the web version of this article.)

playing a role in the transition (Fig. 2) by obstructing the exit of Lys53. As shown in Table S2, interactions are dynamic and partially interrupted during the MD simulations. However, when Lys53 is protonated, these interactions are less frequent by 19–25%, suggesting that protonation is correlated with the disruption of the H-bond network close to Lys53, which in turn can facilitate the transition to the "out" conformation.

Fig. 3 compares the evolution of selected interactions in the vicinity of the decoordinated Lys53 in WT THB1. When Lys53 is neutral (Fig. 3A), interactions between Lys49 and Arg52 and the heme propionates fluctuate, but Lys53 Nζ remains relatively close to the heme iron (~3 Å). However, when Lys53 is protonated in the cavity, the fluctuations depict the 5c-in → 5c-out transition. Initially, Lys53H$^+$ shows a 5c-in conformation evidenced by a Fe–Nζ distance of ~6 Å, and residues Lys49 and Arg52 maintain loose, fluctuating interactions with the heme propionates. Lys53H$^+$ begins its exit when neither Lys49 nor Arg52 interacts with heme propionates. Arg52 then returns to its initial position and establishes a stable interaction with the heme 7-propionate for the rest of the time scale of the MD simulation whereas the interaction between Lys49 and the heme 6-propionate is completely lost. Finally, a new interaction between Lys53H$^+$ and the heme 6-propionate, represented by the distance between Lys53 Nζ and the carboxylate carbon (CGD), is established. Altogether, the movement of these three residues triggers the displacement of the E helix (Fig. 2C). The final 5c-out conformation accessed by the MD simulations here, however, does not superimpose exactly with the "out" conformation represented by the crystallographic structure of cyanide-bound THB1 (Fig. 1B), in which the E helix fully rotates about its long axis and introduces residues Gln50 and Gln54 into the distal heme pocket. As a control, MD simulations for 5c WT-Lys and WT-LysH$^+$ were extended up to 3 μs, with results similar to those observed in the shorter simulations (Fig. S4).

3.1.2. MD simulations of Ala variants

In order to investigate the importance of Lys49 and Arg52, 300 ns of MD simulations were performed with Lys49Ala (K49A), Arg52Ala (R52A) and Lys49Ala/Arg52Ala (K49A/R52A, or AA) THB1 after in silico replacement and equilibration. With each of the single Ala replacements (Fig. S5), we observed a behavior similar to that of WT THB1 (Fig. 3): Lys53 in the neutral state does not spontaneously exit the cavity, while protonated Lys53 exits after 200 ns (K49A THB1) and 10 ns (R52A THB1). Interestingly, interactions between the heme propionates and Lys49 or Arg52 in the single variants are not weakened when Lys53 is protonated. Additionally, interactions are reinforced with respect to the interactions observed in the WT protein (Table S2).

Of note, in the double variant (AA THB1, Fig. S5), the transition occurs spontaneously in both Lys53 protonation states indicating that the absence of both steric hindrance and attractive interactions between residues at positions 49 and 52 with the propionates allows the neutral Lys53 to leave the distal cavity. In fact, in the WT simulations, the correlation of the Nζ(Lys53)–Fe(heme) distance with Nζ(Lys49)–CGD (heme) and Cζ(Arg52)–CGA(heme) for WT THB1 (Fig. S6) shows that in order for Lys53 Nζ to increase its distance from Fe and exit the heme cavity, the Nζ(Lys49)–CGD(heme) and Cζ(Arg52)–CGA(heme) interactions have to be broken simultaneously. The figure also illustrates the distinct effect of individual Ala replacements.

It is noteworthy that in all simulations (WT and variants, 6c and 5c states), we observed the presence of water molecules in the heme cavity. This phenomenon was further quantified as the percentage of simulation time when one or more water molecules were found within 5 Å of the buried Lys53 Nζ (Fig. S7). Such observation, contrasting with an assessment of the static crystallographic structure alone, suggests that the heme pocket is not fully protected from solvent and that interaction of water molecules with Lys53 can occur inside the distal cavity. Closer

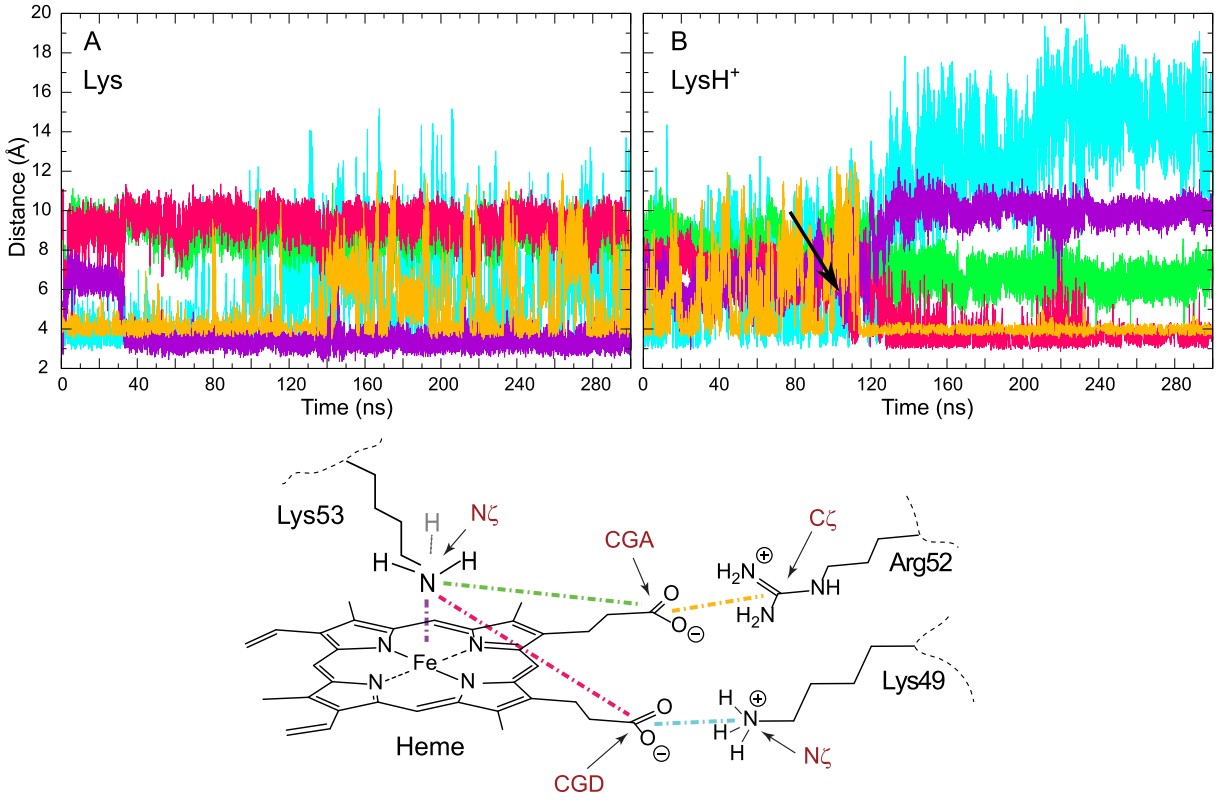

Fig. 3. Interactions in the vicinity of Lys53 in THB1 in-out transition from MD simulations starting in the 5c-in state. A) WT-Lys and B) WT-LysH$^+$ as a function of time. Distances between the Lys53 Nζ and Fe of heme, the Arg52 Cζ and the heme 7-propionate Cγ (CGA), the Lys49 Nζ and the heme 6-propionate Cγ (CGD), and the Lys53 Nζ and heme CGA and CGD, are depicted using purple, orange, cyan, green, and red lines, respectively. The black arrow in panel B points out the start of the 5c-in → 5c-out transition. (For interpretation of the references to colour in this figure legend, the reader is referred to the web version of this article.)

inspection of the trajectories revealed that specific distal residues allow the hydration of the heme cavity throughout the duration of the simulations. In most cases, Tyr29 (B10) points its phenol hydroxyl group inward and Gln50 (E7) rotates its side chain amide away from the protein–solvent interface and toward Lys53. These alternative rotameric states increase the polarity of the heme pocket and form a narrow channel opening at the interface of the B, C, and E helices, which allow a continuous chain of water molecules to solvent (Fig. S8).

3.2. Decoordination and protonation of Lys53 studied by hybrid QM/MM calculations

As a prerequisite of the Lys53 5c–in → 5c–out transition investigated above, the cleavage of the Fe–Lys53 bond needs to be considered. Because this process involves the rupture of a chemical bond, a hybrid QM/MM approach was applied. By using these restricted optimizations, we intended to explore possible mechanisms for Fe–Lys53 bond breaking and the occurrence of Lys53 protonation during or after the process, features that cannot be readily determined by experimental methods.

It is important to consider that the overall decoordination reaction involves a spin transition, from a low-spin, 6c state ($S = 0$, singlet state for Fe(II)) to a high-spin, 5c state ($S = 2$, quintuplet state for Fe(II)), of which the latter was apparently not detected in the NMR lineshape experiments relying on the NH_2 group. All systems considered below were calculated in three different spin states: singlet, triplet and quintuplet for Fe(II), in order to consider all possibilities along the transition. It has been previously shown that some DFT functionals disfavor the stabilization of higher multiplicity states [56,57]. For that reason, we will center our analysis on the general shape of the potential energy surfaces and discuss qualitative trends associated with the processes.

The first attempt to obtain the 5c state from the 6c state was performed by slowly pulling Lys53 away from the iron and the heme group along the direction of the Fe–Nζ bond. In this case, the QM subsystem consisted of the heme group (excluding the macrocycle substituents) plus the axial ligands: the imidazole ring of His77 coordinated by the Nε2 atom and the side chain of Lys53. The chosen reaction coordinate in this case was the distance between Nζ of Lys53 and the Fe atom, from 2.04 to 6.00 Å.

Fig. 4 illustrates the evolution of Lys53 side chain geometries involved in the process for the Fe(II) singlet state, showing that while Lys53 moves away from Fe, the Nζ–Cε bond rotates and the H–N–H angle is kept almost constant along the reaction (moving from ~104° to ~106.5°). As can be observed in the energy profile (Fig. S9), no stable minimum is obtained for this reaction coordinate in any of the three spin states. Additionally, in the singlet state, which corresponds to the 6c ground energy state, a rapid increase in the potential energy is observed when the Fe-Lys53 bond is elongated. This increase in system energy and lack of a stable minimum in the 5c state shows that the decoordination of neutral Lys53 is unfavorable.

As an alternative for the neutral decoordination reaction, we studied the possibility of a concerted Fe–Lys53 bond cleavage and Lys53 protonation. For this purpose, we modified the QM region so that it would consist of the heme group, the same axial ligands as above, and a water-hydronium pair (or Zundel cation, $H_5O_2^+$) near the Lys53 Nζ (Fig. 5). The inclusion of these solvent molecules was considered mechanistically feasible because of the observation along the MD simulations of continuous hydrogen-bonded waters connecting the distal heme cavity to bulk solvent (Fig. S8). The position and number of water molecules for this analysis were decided on the basis of the solvent conformations with water molecules near Lys53 that were sampled the most during the MD simulation. In this case, the reaction coordinate was selected as the distance between Lys53 Nζ and the closest hydrogen atom molecule. The distance changes from ~3.4 to 1.1 Å during the calculations.

As can be observed in the resulting energy profile (Fig. S10), a clear and stable minimum with Lys53 decoordinated and protonated was achieved, the result being similar for the three spin states. In this system, the ΔE obtained for each spin state was −7, −27, and −25 kcal/mol for the singlet, triplet and quintuplet states, respectively.

Relevant Lys53 side chain geometries along the concerted protonation/decoordination process are shown in Fig. 5, including structures for the initial complex, transition state and product in the Fe(II) oxidation state. The reaction initiates with Lys53 moving away from Fe with the neutral amino group becoming increasingly planar as it progresses through the reaction coordinate, contrary to the mechanism depicted in Fig. 4A. The water molecule near the Nζ acts as a H-bond donor, while the Fe–Nζ bond is elongated compared to the initial state. At the same time, this water molecule shares another proton with a second nearby water molecule. Once the transition state is passed, the Lys53 H–Nζ–H angle returns to its original value, and the reactive water shares the proton with Lys53. Inversion of the Lys53 amino group is accompanied by a sudden increase in the Fe–Lys distance. Further along the path, as Lys53 keeps moving away from the iron, the water molecule finally transfers a proton to the amino group and accepts a proton from the second water molecule. These results show that, at least computationally, the concerted protonation/decoordination mechanism is more energetically favorable than the "dry" decoordination mechanism alone.

3.3. Summary of the computational results

Overall, the calculations provide insight into the feasibility of different 6c → 5c-out mechanisms. QM/MM calculations reveal an energetically favorable path for protonation of the amino group within the heme pocket, and MD simulations suggest that the presence of a

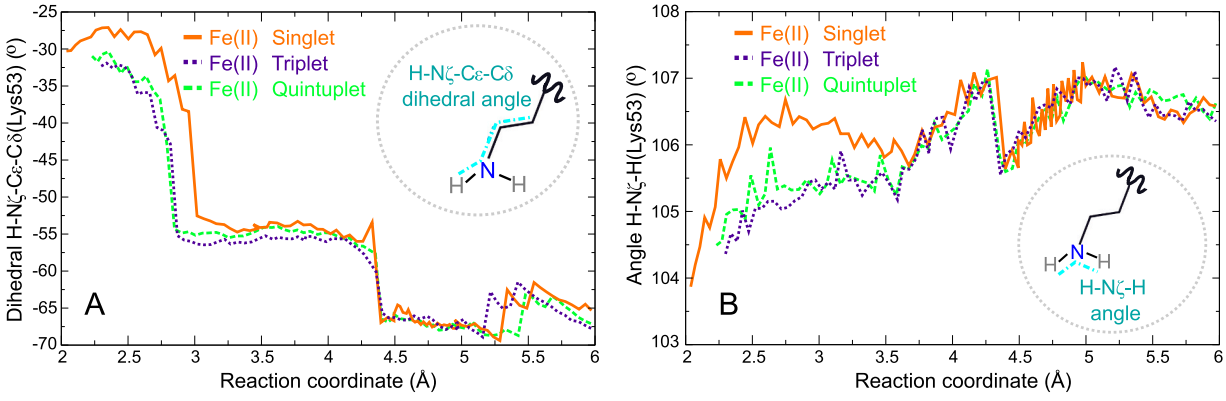

Fig. 4. Selected geometrical parameters involved in Lys53 decoordination from heme along the reaction coordinate for Fe(II) for the three spin states. The reaction coordinate is the distance between Nζ of Lys53 and Fe of heme. A) Lys53 Cδ–-Cε–Nζ–H dihedral angle. B) Lys53 H–Nζ–H angle in the amino group.

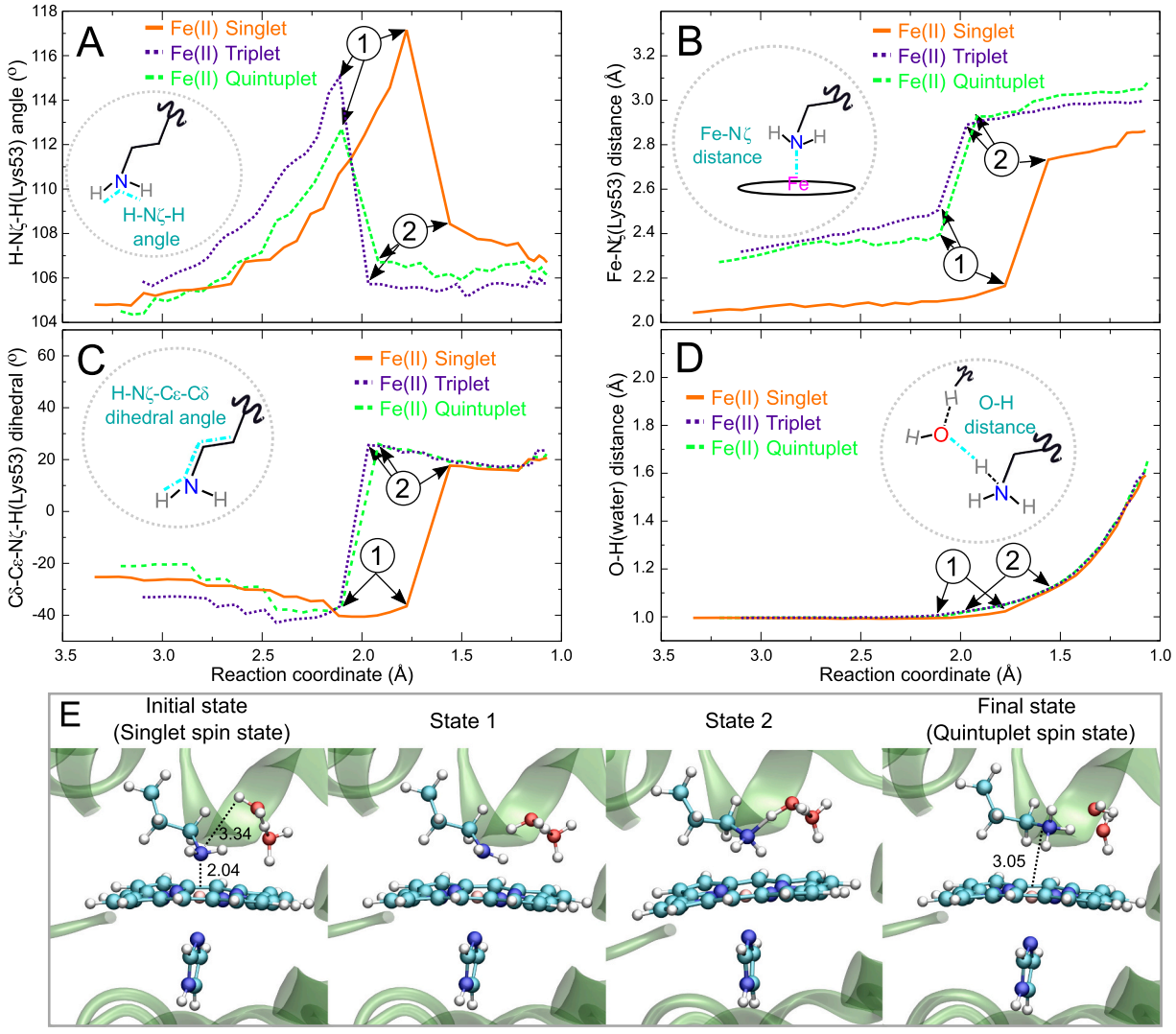

Fig. 5. Selected geometrical parameters involved in the concerted protonation/decoordination mechanism of Lys53 in Fe(II) THB1 for the three spin states considered. The reaction coordinate is the distance between the reacting water proton and the Lys53 Nζ. A) Lys53 H–Nζ–H angle in the amino group, B) Fe–Nζ (Lys53) distance, C) Lys53 Cδ–Cε–Nζ–H dihedral angle, and D) O–H distance of the nearest water to Lys53. E) Typical snapshots representing the initial state, two states along the reaction path, representing the state before and after the water molecule donates the proton to Lys53 (State 1 and 2, respectively), and the final state. States 1 and 2 are highlighted in A–D.

buried, ionized Lys53 headgroup drives the expulsion of the side chain to the solvent where it can interact with the negatively charged heme propionates. A water-hydronium pair was explicitly included in our QM/MM calculations to mirror the solvation pattern observed in the MD results. In addition, the side chain replacements of Lys49 and Arg52 to Ala play a role in controlling the likelihood that the rearrangement will take place, with Arg52 the more important of the two residues.

3.4. pH dependence of heme axial coordination in K49A, R52A and K49A/R52A THB1

In a parallel experimental study [25], we have shown how modifications at the heme periphery can affect the apparent pK_a of the transition from neutral and coordinated Lys53 to charged and decoordinated Lys53 in the Fe(II) and Fe(III) state of THB1. Absent from that study were Ala replacements at positions 49 and 52. With the goal to connect computational and experimental results, we prepared K49A, R52A and K49A/R52A (AA) THB1 and examined the 6c → 5c-out transition of these Ala variants induced by low pH. For reference, the apparent pK_as of the transition measured for Fe(II) and Fe(III) WT THB1 [18] are listed in Table 1, ~6.6 and 6.5, respectively. In the Fe(III) state, the absorption

Table 1
Apparent pK_a values and Hill coefficients for the pH response of THB1 and variants.

	Fe(III)		Fe(II)	
	His/H_2O ⇌ His/Lys		−/− & His/− ⇌ His/Lys	
	pK_a	*n*	pK_a	*n*
WT	6.48 ± 0.07[a]	0.86 ± 0.03[a]	~6.6[a,b]	ND
K49A	6.76 ± 0.02	0.69 ± 0.02	7.70 ± 0.06	0.80 ± 0.07
R52A	6.97 ± 0.02	0.71 ± 0.03	7.86 ± 0.03	0.85 ± 0.04
K49A/R52A	7.35 ± 0.01	0.81 ± 0.02	8.47 ± 0.04	0.96 ± 0.08
K49E[b]	8.39 ± 0.01	0.84 ± 0.02	9.02 ± 0.03	1.03 ± 0.07
R52E[b]	7.71 ± 0.02	0.75 ± 0.02	8.24 ± 0.03	0.81 ± 0.04
K49E/R52E[b]	9.19 ± 0.01	0.91 ± 0.01	9.68 ± 0.03	0.86 ± 0.06

Values determined by SVD and global fitting of absorbance data collected at room temperature.
ND, not determined.
[a] From [18].
[b] Glu variant data from [25].

spectra of the variants were consistent with Lys coordination at high pH and water coordination at low pH. The spectra of reduced states at both pH extremes also resembled closely the corresponding WT spectra. As noted in prior work, the apparent pK_a value in the Fe(II) state is determined less accurately than in the Fe(III) because of complications associated with the chemical instability of the reduced species and the contribution of an additional species, likely tetracoordinate (4c), at low pH. Structurally, the transitions in the two oxidation states differ in that in the Fe(II) state, the Lys-off state is a 5c complex, whereas in the Fe(III) state, a water molecule replaces Lys53. By analogy to other TrHbs, the water-bound state (aquomet) is assumed to have the same polypeptide conformation as the cyanide-bound state (cyanomet, PDB ID 6CII). The apparent pK_a values for the three Ala variants are listed in Table 1, along with the related Glu variants [25]. Representative data are shown in Fig. 6 and full titrations are shown in Fig. S11 and Fig. S12.

Compared to WT THB1, a small (< 1 pH unit) increase in apparent pK_a is observed for all Ala variants in the Fe(III) state and a greater increase in the Fe(II) state. In both oxidation states, the Arg52 replacement has a slightly larger effect than the Lys49 replacement. This contrasts with the effect of charge reversals at the same positions. For these, the increase in pK_a is larger and the influence of position 49 surpasses that of position 52. The shift in pK_a of the AA variant is less than the sum of the effects caused by the single variants. Non-additivity is obvious in the Fe(II) state and shows that replacing the second residue in the background of the first replacement results in a modest increase in net 6c destabilization.

4. Discussion

4.1. Positively charged side chains in the distal heme pocket of globins

The distal environment of the heme group is a natural focus of hemoglobin studies because of its dominant role in setting ligand binding kinetics and heme reactivity. In the canonical globin fold represented by Mb, E7 is the topological equivalent of THB1's E10 and is often occupied by a histidine located at a non-coordinating distance from the iron, positioned to stabilize exogenous ligands through hydrogen bonding [58]. At low pH (< 5), His E7 undergoes protonation and rotates toward solvent [59], opening a gate to the distal site. For THB1, lowering the pH also appears to result in the expulsion of the charged distal residue (Lys E10). In a related example, the β subunit of hemoglobin Zürich, which has an arginine at E7, adopts a conformation by which the positive headgroup interacts with a heme propionate [60], much as the displaced Lys E10 investigated here.

Contrasting with the expulsion of a charged group from the distal site, some Mb-like proteins lacking His E7 stabilize the exogenous ligand with an arginine at E10. For example, *Aplysia limacina* Mb [61], *Dolabella auricularia* Mb [62], and artificial variants of sperm whale Mb [63] accommodate the charged guanidino group within the hydrophobic distal cavity at the cost of a modest conformational deviation from the parent Mb structure. *Propsilocerus akamusi* Hb V, on the other hand, shows a pH-dependent orientation of Arg E10 with side chain conformations inside and outside of the heme cavity [64]. The TrHb fold, however, appears less constraining than the Mb fold, and ligand stabilization generally occurs with the B10-E7-E11 trio of residues [6]. For THB1, this triad offers a more stable alternative than interactions solely between distal lysine and exogenous ligand. Unlike Hb Zürich, Lys53Arg THB1 populates the hydroxide-bound Fe(III) protein at neutral pH [65], a manifestation that the ligand interactions with arginine outcompete the TrHb triad.

The combination of lysine coordination and decoordination, proton binding, ligand switching, and conformational rearrangement shows THB1 to be a complex system sharing the properties of disparate Mb-like proteins but particularly challenging for a mechanistic study. Previous NMR spectroscopy measurements of THB1 at equilibrium sought to explain the behavior of Lys53 and fleshed out a dynamic basis tied to this protein's purported role in the cell as an NOD enzyme (or more generally one that binds a substrate at the iron center). It also laid bare gaps in the detailed understanding of lysine (de)coordination. In this work, we attempted to explore plausible molecular mechanisms for the complete 6c → 5c-out transition of WT THB1. In order to accomplish this goal, we have applied a combination of classical and hybrid QM/MM calculations

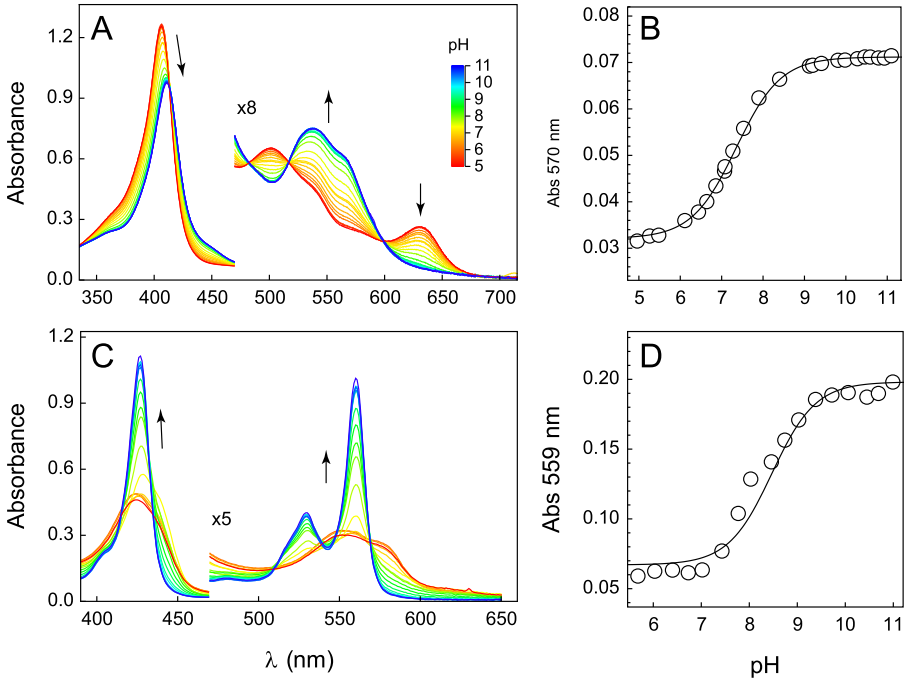

Fig. 6. pH titrations of THB1 K49A/R52A monitored by electronic absorption spectroscopy. A–B) Fe(III) data with apparent pK_a of 7.35 ± 0.01. C–D) Fe(II) data with apparent pK_a of 8.47 ± 0.04. The colour pH legend is shared by both spectra, and the arrows indicate spectral changes with increasing pH. On the right panels, the single-wavelength data is fitted using globally determined parameters (Fig. S11 for Fe(III), S12 for Fe(II), and Table 1).

accompanied by experimental work.

4.2. Computational representation of Lys E10 decoordination

A reasonable set of microstates that connect the observable heme coordination states in THB1 is shown in Scheme 2 (adapted from [25]) and serves as a theoretical basis for understanding the experimental and computational results presented in this work. The MD simulations capture the exit of Lys53 and the adoption of a stable conformation outside of the heme cavity (Scheme 2C). They also reveal that this transition is favored when Lys53 is protonated inside the distal cavity (Scheme 2B). Although these simulations do not pinpoint the exact reaction coordinate position at which Lys53 gets protonated, the trajectories strongly suggest that, if this process occurs in the vicinity of the iron, it ensures progress toward side chain exit rather than recoordination. Decoordination/recoordination is indeed apparent in NMR linewidth measurements when the proton concentration is low [26]. The MD results of WT THB1 and selected variants also indicate that the heme propionates, in their interactions with Lys49 and Arg52, play a key role in stabilizing lysine coordination (Scheme 2A). When these basic residues interact with the heme propionates, they form a cage-like structure, likely helping to stabilize the E helix and making it more energetically difficult for Lys53 to exit the heme cavity. The simulations support the need for removing both interactions in order to facilitate the conformational transition.

Other features inherent in the conformational change aside from protein–heme interactions (e.g., exogenous ligand binding, interhelical hydrophobic packing, loop flexibility, etc.) could also be expected to play important roles in the transition. In fact, while the movements of Lys49, Lys53 and Arg52 induce a displacement of the E helix from its initial conformation, the final simulated structure does not overlap perfectly with that of the cyanomet complex (compare Fig. 1B and Fig. 2B). It is possible that the exogenous ligand, with its own set of interactions, enhances the driving force for Tyr29, Gln50 and Gln54 to turn into the cavity and promote further rotation of the E helix. The absence of exogenous ligand and a high activation barrier due to the reorganization of interhelical contacts [25] may explain the difference between the final simulated structure and the cyanomet complex. Nevertheless, the simulations do show the repositioning of Lys53 to the protein exterior, which suggests that other features, specifically those involving the heme propionates, are reliably predicted.

The QM/MM calculations predict passage through a transition state where the Fe–Lys53 coordination bond is elongated. While Lys53 is still close to Fe, Lys53 can accept a proton from a nearby water molecule. The MD simulations show that water molecules, assisted by distal polar residues Tyr29 and Gln50, are able to form a continuous, hydrogen-bonded chain between bulk solvent and the distal side, a development that would make the protonation step feasible (Scheme 2, A to B). Accepting this proton significantly reduces the energy barrier for bond breaking, resulting in an energetically favored, concerted transition to the protonated 5c-in state. Finally, a favorable transition to the 5c-out state can occur (Scheme 2, B to C), as observed in the classical MD simulations.

The NMR characterization of WT Fe(II) THB1 in solution [26] did not indicate the presence of ordered water molecule(s) in the distal pocket. However, evidence for transient water penetration was obtained with water-presaturation and nuclear Overhauser experiments at high pH, where the 6c state is fully populated. Furthermore, lineshape analysis of Lys 53 NH_2 and results obtained under variable solvent isotopic (H_2O:D_2O) composition are consistent with rapid and reversible decoordination, followed by a rotation/inversion motion of the amino group. Interestingly, the QM/MM calculations can accommodate this mechanism. Lys53 is able to decoordinate from Fe but, as shown in Fig. S9, an energy minimum does not correspond to the resulting 5c state unless the

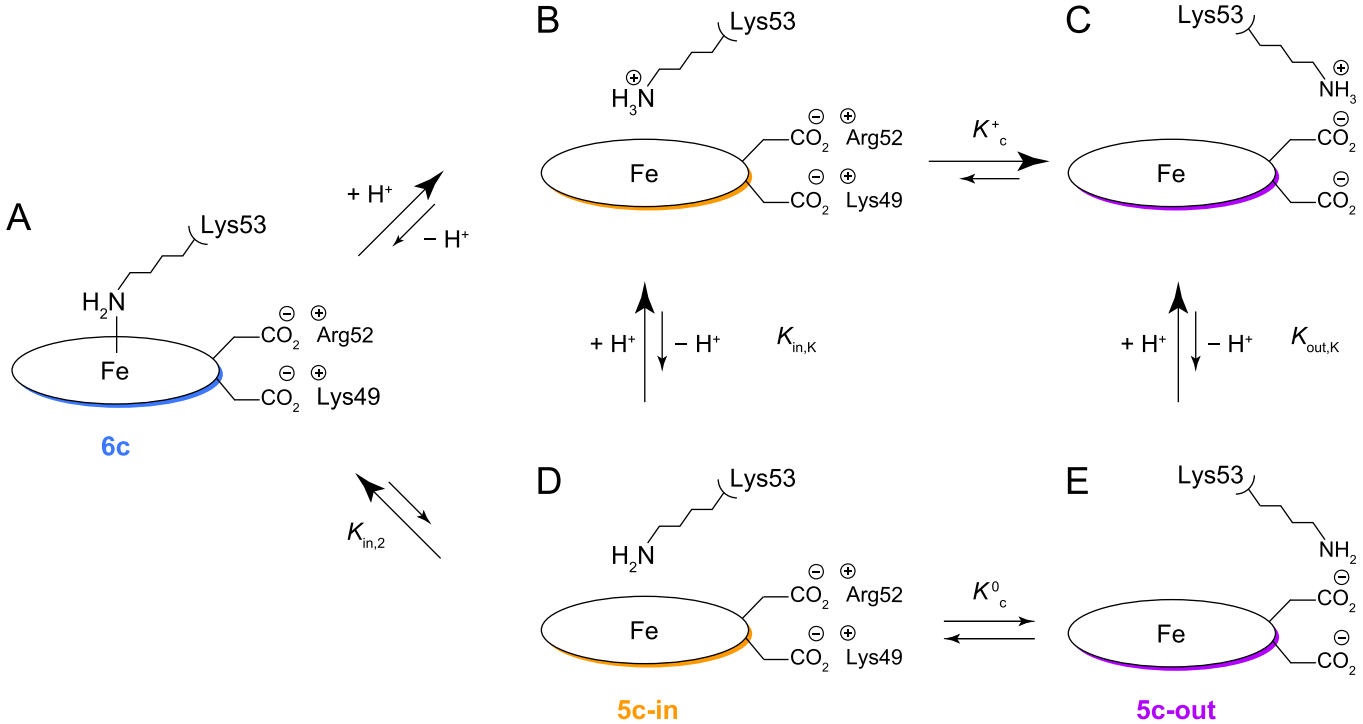

Scheme 2. Microstates discussed in this work (proximal histidine omitted for clarity). The pH-dependent process followed by electronic absorption spectroscopy involves the equilibrium between 6c and 5c-out, $LysH^+$ (A ⇄ C). Other plausible states include B) the 5c-in, $LysH^+$ state and E) the 5c-out, Lys state. Hybrid QM/MM calculations favor a concerted mechanism involving protonation and decoordination (A ⇄ B), whereas "dry" Lys decoordination (A ⇄ D), does not appear to be energetically likely. MD results show that exit of $LysH^+$ from the heme cavity (B ⇄ C) is preferred over that of Lys (D ⇄ E), and that this process is modulated by ionic interaction with the heme propionates. Internal Lys protonation (D ⇄ B) is feasible given the internal solvation observed by MD, and of course also possible with a solvent-exposed Lys (E ⇄ C). The relevant equilibrium constants are taken from derivations in [25].

amino group is protonated (Fig. S10). At high pH, the probability of Lys53 protonation and exit is low, which allowed for the NMR observations. Under those conditions, a different mechanism may operate and the results from the QM/MM calculations cannot be directly compared to the experimental data.

We have noted that the pK_a shift caused by the double Ala replacement does not correspond to the sum of the individual effects. Although a molecular explanation for this observation cannot be derived from the available data, it is intriguing that the MD simulations allow Lys53 to exit the pocket of AA THB1 while in the neutral state as well as the charged state. This was also seen for K49E and EE THB1 (data not shown). All three variants exhibit an upward shift in pK_a of ~2 pH units or higher in the relevant oxidation state. Thus, it appears that the replacements causing the largest destabilization of the 6c/5c-in state relative to the 5c-out state, as determined by apparent pK_a measurements, produce markedly destabilized 5c-in simulated structures, for which expulsion of a neutral Lys53 now becomes feasible within the timescale explored. This correlation between the experimental and computational data points to the stability of the 5c-in state, aside from any decoordination/protonation mechanism, as an important underlying component to the energetics of the overall 6c → 5c-out transition and the resulting NOD activity of THB1.

4.3. Experimental assessment of Lys49 and Arg52 role in Lys53 decoordination

Eliminating protein–propionate interactions by placing Ala at positions 49 or 52 (or both) raises the apparent pK_a of the 6-c ⇄ 5c-out transition. Table 1 and Fig. S13 show the influence of Ala replacements and contrast it with that of the Glu counterparts. In the Fe(II) state, the apparent pK_as reflect the different electrostatic consequences brought about by the two types of replacements, neutralizing or reversing the charge. In the Fe(III) state, however, a water molecule competes with Lys for coordination, and this additional equilibrium factors into the assessment of energetics [25]. Thus, a combination of water affinity and electrostatic effects evidenced in the Fe(II) state is responsible for the pK_a gap between the Fe(III) and Fe(II) state. The larger gap for the Ala variants may stem from less efficient water competition. It is interesting that the individual Ala and Glu replacements have opposite differential effect on the apparent pK_a; while Ala52 causes a larger shift than Ala49, the reverse is observed for Glu52 and Glu49. This may reflect additional electrostatic effects such as repulsion caused by the proximity of Asp46 (E3) and Glu49. Although details vary from variant to variant, the experimental and computational results support the importance of the positively charged Lys49 and Arg52 in blocking the decoordination of Lys53.

Among a set of 344 group 1 TrHbs (TrHb1s, the branch of TrHbs that contains THB1) [65], the Ala substitution is often found at position E9 when Lys is present at position E10. The combination Lys E10/Ala E9 accounts for ~40% of the proteins with Lys E10, whereas the combination Lys E10/Ala E6 occurs with a frequency lower than 10% [25]. The combination Lys E10/Ala E6/Lys E9 is rare (< 3%). In contrast, Glu is rarely found at positions E6 and E9 when a Lys is at E10 (< 5%, with no example yet with E at both positions). On the basis of the computational and experimental data, we anticipate that among TrHb1s with Lys E10, the simultaneous presence of Asp at E3, Glu at E6, and Ala at E9 will disfavor Lys coordination.

4.4. Proposed mechanism and reconciliation with experimental data

Overall, we can envision at minimum three possibilities for the mechanism of lysine decoordination and THB1 rearrangement:

(1) Decoordination occurs, followed by the exit of the amino headgroup to the solvent, followed by protonation and docking with the heme propionate (Scheme 2, A → D → E → C). The first step in this sequence is unfavorable according to the QM/MM calculations but feasible according to the high-pressure NMR data discussed in [26]. The second step appears unlikely in WT THB1 but is possible if WT interactions involving the heme propionates are perturbed (as observed for AA THB1).

(2) Decoordination occurs, followed by protonation, followed by exit of the protonated amino headgroup to the solvent (Scheme 2, A → D → B → C). The first step in this sequence is again unfavorable according to the QM/MM calculations, but possible according to NMR data collected at high pH. The second step is likely according to MD simulations, which show the reorganization of polar residues into the heme cavity and water penetration. A chain of water molecules and a Grotthuss-like transport mechanism can be invoked for protonation [66]. The last step is readily explained with favorable charge-charge interactions with heme propionates.

(3) Concerted decoordination and protonation followed by exit to solvent (Scheme 2, A → B → C). In this sequence of events, the first step is favored by the QM/MM calculations and plausible because of the MD observation of water penetration in the heme cavity. The third step is favored, as in scenario (2).

Considering the limitations of experimental characterization, MD simulations, and QM/MM calculations, all three scenarios are valid. However, our computational results provide more support to scenarios 2 and 3, owing to the difficulty of stabilizing a neutral, decoordinated Lys53 within the heme cavity and also of moving from the in to out conformation. Precedents for water penetration in relatively hydrophobic heme environments provide support for protonation within the heme cavity. For example, autooxidation is a process common to Hbs, which requires participation of a hydroxyl or hydronium [67–69], often facilitated by distal residues (e.g., His E7). Nitrate release in the NO dioxygenation process of the group 1 TrHb from *Mycobacterium tuberculosis* proceeds by water penetration [70]. In THB1 at neutral pH, our results favor scenario 3, with efficient proton transport facilitated by the motions of polar residues in the distal pocket. The concerted mechanism, however, requires further experimental confirmation given the apparent hydrophobicity of the heme environment in THB1.

5. Conclusion

As a likely NOD enzyme, WT THB1 must cycle the coordination state of the distal lysine. The available X-ray structures, the pH lability of the distal Fe–Lys bond, and the lysine dynamics studied by NMR spectroscopy raised a specific mechanistic question that was approached first with MD simulations. The trajectories suggested that expulsion of the decoordinated Lys53 to solvent was facilitated when in the positively charged state and when interactions between neighboring Lys49 and Arg52 with the heme propionates were broken. Hydration of the distal cavity and formation of a water chain to solvent, a key feature of the MD simulations, opened the possibility of protonation along the transition. Hybrid QM/MM calculations showed the plausibility of a concerted protonation and decoordination of Lys53. Overall, the studies presented here and in the accompanying paper [25] offer original insights into heme axial coordination by a lysine amino nitrogen. They highlight the profound influence of nearby amino acids, secondary structure of adjacent polypeptide segments, and solvation of the heme cavity on the physico-chemical properties of the protein. They also emphasize the synergy of computational and experimental investigation necessary for understanding the behavior of hemoglobins with unusual coordination schemes.

Abbreviations

4c	four-coordinate

(continued on next page)

(*continued*)

5c	five-coordinate
6c	six-coordinate
DFT	density functional theory
AA THB1	K49A/R52A THB1
Hb	hemoglobin
Mb	myoglobin
NOD	nitric oxide dioxygenase
PDB	Protein Data Bank
QM/MM	quantum mechanics-molecular mechanics
RMSD	root-mean-square deviation
RMSF	root-mean-square fluctuation
SVD	singular value decomposition
TrHb	truncated hemoglobin
TrHb1	group 1 truncated hemoglobin
WT	wild-type

Declaration of Competing Interest

The authors declare that they have no known competing financial interests or personal relationships that could have appeared to influence the work reported in this paper.

Acknowledgments

This research was supported by grants from the Universidad de Buenos Aires (UBACYT 20020120300025BA), Agencia Nacional de Promoción Científica y Tecnológica (PICT 2016-0568, PICT 2014-1022, and PICT 2015-2761) and CONICET Grant 11220150100303CO. L.J.P. holds a CONICET PhD fellowship. D.A.E. and L.C. are members of CONICET. Support was also provided by the National Science Foundation grant numbers MCB-1330488 and CHE-2003950 to JTJL and GRFP-1746891 to JEMG. The authors thank Dr. Matthew Preimesberger for initiating the analysis of Lys53 dynamics and useful discussion, and Dr. Eric Johnson for assistance in molecular biology steps and protein preparation as well as discussion of the results.

Appendix A. Supplementary data

Supplementary data to this article can be found online at https://doi.org/10.1016/j.jinorgbio.2021.111455.

References

[1] S.N. Vinogradov, M. Tinajero-Trejo, R.K. Poole, D. Hoogewijs, Bacterial and archaeal globins — A revised perspective, Biochim. Biophys. Acta 1834 (2013) 1789–1800, https://doi.org/10.1016/j.bbapap.2013.03.021.

[2] S.N. Vinogradov, X. Bailly, D.R. Smith, M. Tinajero-Trejo, R.K. Poole, D. Hoogewijs, Microbial eukaryote globins, Adv. Microb. Physiol. 63 (2013) 391–446, https://doi.org/10.1016/B978-0-12-407693-8.00009-1.

[3] S.N. Vinogradov, I. Fernandez, D. Hoogewijs, R. Arredondo-Peter, Phylogenetic relationships of 3/3 and 2/2 hemoglobins in Archaeplastida genomes to bacterial and other eukaryote hemoglobins, Mol. Plant 4 (2011) 42–58, https://doi.org/10.1093/mp/ssq040.

[4] J.B. Wittenberg, M. Bolognesi, B.A. Wittenberg, M. Guertin, Truncated hemoglobins: a new family of hemoglobins widely distributed in bacteria, unicellular eukaryotes and plants, J. Biol. Chem. 277 (2002) 871–874, https://doi.org/10.1074/jbc.R100058200.

[5] D.A. Vuletich, J.T.J. Lecomte, A phylogenetic and structural analysis of truncated hemoglobins, J. Mol. Evol. 62 (2006) 196–210, https://doi.org/10.1007/s00239-005-0077-4.

[6] A. Pesce, M. Couture, S. Dewilde, M. Guertin, K. Yamauchi, P. Ascenzi, L. Moens, M. Bolognesi, A novel two-over-two a-helical sandwich fold is characteristic of the truncated hemoglobin family, EMBO J. 19 (2000) 2424–2434, https://doi.org/10.1093/emboj/19.11.2424.

[7] P. Arroyo Manez, C. Lu, L. Boechi, M.A. Martí, M. Shepherd, J.L. Wilson, R. K. Poole, F.J. Luque, S.R. Yeh, D.A. Estrin, Role of the distal hydrogen-bonding network in regulating oxygen affinity in the truncated hemoglobin III from *Campylobacter jejuni*, Biochemistry 50 (2011) 3946–3956, https://doi.org/10.1021/bi101137n.

[8] A. Lama, S. Pawaria, A. Bidon-Chanal, A. Anand, J.L. Gelpí, S. Arya, M. Martí, D. A. Estrin, F.J. Luque, K.L. Dikshit, Role of pre-a motif in nitric oxide scavenging by truncated hemoglobin, HbN, of *Mycobacterium tuberculosis*, J. Biol. Chem. 284 (2009) 14457–14468, https://doi.org/10.1074/jbc.M807436200.

[9] A. Bidon-Chanal, M.A. Martí, D.A. Estrin, F.J. Luque, Dynamical regulation of ligand migration by a gate-opening molecular switch in truncated hemoglobin-N from *Mycobacterium tuberculosis*, J. Am. Chem. Soc. 129 (2007) 6782–6788, https://doi.org/10.1021/ja0689987.

[10] Y. Ouellet, M. Milani, M. Couture, M. Bolognesi, M. Guertin, Ligand interactions in the distal heme pocket of *Mycobacterium tuberculosis* truncated hemoglobin N: roles of TyrB10 and GlnE11 residues, Biochemistry. 45 (2006) 8770–8781, https://doi.org/10.1021/bi060112o.

[11] A. Bidon-Chanal, M.A. Martí, A. Crespo, M. Milani, M. Orozco, M. Bolognesi, F. J. Luque, D.A. Estrin, Ligand-induced dynamical regulation of NO conversion in *Mycobacterium tuberculosis* truncated hemoglobin-N, Proteins: Struct. Funct. Bioinf. 64 (2006) 457–464, https://doi.org/10.1002/prot.21004.

[12] A. Crespo, M.A. Martí, S.G. Kalko, A. Morreale, M. Orozco, J.L. Gelpi, F.J. Luque, D. A. Estrin, Theoretical study of the truncated hemoglobin HbN: exploring the molecular basis of the NO detoxification mechanism, J. Am. Chem. Soc. 127 (2005) 4433–4444, https://doi.org/10.1021/ja0450004.

[13] N.L. Scott, Y. Xu, G. Shen, D.A. Vuletich, C.J. Falzone, Z. Li, M. Ludwig, M.P. Pond, M.R. Preimesberger, D.A. Bryant, J.T.J. Lecomte, Functional and structural characterization of the 2/2 hemoglobin from *Synechococcus* sp. PCC 7002, Biochemistry 49 (2010) 7000–7011, https://doi.org/10.1021/bi100463d.

[14] M.R. Preimesberger, M.P. Pond, A. Majumdar, J.T.J. Lecomte, Electron self-exchange and self-amplified posttranslational modification in the hemoglobins from *Synechocystis* sp. PCC 6803 and *Synechococcus* sp. PCC 7002, J. Biol. Inorg. Chem. 17 (2012) 599–609, https://doi.org/10.1007/s00775-012-0880-5.

[15] M.R. Preimesberger, A. Majumdar, S.L. Rice, L. Que, J.T.J. Lecomte, Helix-capping histidines: diversity of N-H...N hydrogen bond strength revealed by $^{2h}J_{NN}$ scalar couplings, Biochemistry 54 (2015) 6896–6908, https://doi.org/10.1021/acs.biochem.5b01002.

[16] A.N. Hvitved, J.T. Trent III, S.A. Premer, M.S. Hargrove, Ligand binding and hexacoordination in *Synechocystis* hemoglobin, J. Biol. Chem. 276 (2001) 34714–34721, https://doi.org/10.1074/jbc.M105175200.

[17] E.A. Johnson, J.T.J. Lecomte, Characterization of the truncated hemoglobin THB1 from protein extracts of *Chlamydomonas reinhardtii*, F1000Research 3 (2014) 294, https://doi.org/10.12688/f1000research.5873.1.

[18] E.A. Johnson, S.L. Rice, M.R. Preimesberger, D.B. Nye, L. Gilevicius, B.B. Wenke, J. M. Brown, G.B. Witman, J.T.J. Lecomte, Characterization of THB1, a *Chlamydomonas reinhardtii* truncated hemoglobin: linkage to nitrogen metabolism and identification of lysine as the distal heme ligand, Biochemistry. 53 (2014) 4573–4589, https://doi.org/10.1021/bi5005206.

[19] P.R. Gardner, Hemoglobin: a nitric-oxide dioxygenase, Scientifica. 2012 (2012) 34, https://doi.org/10.6064/2012/683729.

[20] E. Sanz-Luque, F. Ocaña-Calahorro, A. de Montaigu, A. Chamizo-Ampudia, A. Llamas, A. Galvan, E. Fernández, THB1, a truncated hemoglobin, modulates nitric oxide levels and nitrate reductase activity, Plant J. 81 (2015) 467–479, https://doi.org/10.1111/tpj.12744.

[21] E. De Marinis, L. Casella, C. Ciaccio, M. Coletta, P. Visca, P. Ascenzi, Catalytic peroxidation of nitrogen monoxide and peroxynitrite by globins, IUBMB Life 61 (2009) 62–73, https://doi.org/10.1002/iub.149.

[22] P.R. Gardner, Nitric oxide dioxygenase function and mechanism of flavohemoglobin, hemoglobin, myoglobin and their associated reductases, J. Inorg. Biochem. 99 (2005) 247–266, https://doi.org/10.1016/j.jinorgbio.2004.10.003.

[23] L.A. Carabet, M. Guertin, P. Lagüe, G. Lamoureux, Mechanism of the nitric oxide dioxygenase reaction of *Mycobacterium tuberculosis* hemoglobin N, J. Phys. Chem. B 121 (2017) 8706–8718, https://doi.org/10.1021/acs.jpcb.7b06494.

[24] S. Kakar, F.G. Hoffman, J.F. Storz, M. Fabian, M.S. Hargrove, Structure and reactivity of hexacoordinate hemoglobins, Biophys. Chem. 152 (2010) 1–14, https://doi.org/10.1016/j.bpc.2010.08.008.

[25] J.E. Martinez Grundman, L. Julió Plana, J.L. Schlessman, L. Capece, D. Estrin, J.T. J. Lecomte, Control of distal lysine coordination in a monomeric hemoglobin: a role for heme peripheral interactions, J. Inorg. Biochem. (2021), https://doi.org/10.1016/j.jinorgbio.2021.111437 in press.

[26] M.R. Preimesberger, A. Majumdar, J.T.J. Lecomte, Dynamics of lysine as a heme axial ligand: NMR analysis of the *Chlamydomonas reinhardtii* hemoglobin THB1, Biochemistry. 56 (2017) 551–569, https://doi.org/10.1021/acs.biochem.6b00926.

[27] S.L. Rice, L.E. Boucher, J.L. Schlessman, M.R. Preimesberger, J. Bosch, J.T. J. Lecomte, Structure of *Chlamydomonas reinhardtii* THB1, a group 1 truncated hemoglobin with a rare histidine-lysine heme ligation, Acta Crystallogr. F Struct. Biol. Commun. 71 (2015) 718–725, https://doi.org/10.1107/S2053230X15006949.

[28] D.A. Case, R.M. Betz, D.S. Cerutti, T.E. Cheatham, T.A. Darden, R.E. Duke, T. J. Giese, H. Gohlke, A.W. Goetz, N. Homeyer, S. Izadi, P. Janowski, J. Kaus, A. Kovalenko, T.S. Lee, S. LeGrand, P. Li, C. Lin, T. Luchko, R. Luo, B. Madej, D. Mermelstein, K.M. Merz, G. Monard, H. Nguyen, H.T. Nguyen, I. Omelyan, A. Onufriev, D.R. Roe, A. Roitberg, C. Sagui, C.L. Simmerling, W.M. Botello-Smith, J. Swails, R.C. Walker, J. Wang, R.M. Wolf, X. Wu, L. Xiao, P.A. Kollman, AMBER 2016, University of California, San Francisco, 2016.

[29] L. Capece, M.A. Martí, A. Bidon-Chanal, A. Nadra, F.J. Luque, D.A. Estrin, High pressure reveals structural determinants for globin hexacoordination: neuroglobin and myoglobin cases, Proteins: Struct. Funct. Bioinf. 75 (2009) 885–894, https://doi.org/10.1002/prot.22297.

[30] U.N. Morzan, L. Capece, M.A. Marti, D.A. Estrin, Quaternary structure effects on the hexacoordination equilibrium in rice hemoglobin rHb1: insights from molecular dynamics simulations, Proteins: Struct. Funct. Bioinf. 81 (2013) 863–873, https://doi.org/10.1002/prot.24245.

[31] L. Capece, M.A. Martí, A. Crespo, F. Doctorovich, D.A. Estrin, Heme protein oxygen affinity regulation exerted by proximal effects, J. Am. Chem. Soc. 128 (2006) 12455–12461, https://doi.org/10.1021/ja0620033.
[32] J.-P. Ryckaert, G. Ciccotti, H.J.C. Berendsen, Numerical integration of the cartesian equations of motion of a system with constraints: molecular dynamics of n-alkanes, J. Comput. Phys. 23 (1977) 327–341, https://doi.org/10.1016/0021-9991(77)90098-5.
[33] X. Wu, B.R. Brooks, E. Vanden-Eijnden, Self-guided Langevin dynamics via generalized Langevin equation, J. Comput. Chem. 37 (2016) 595–601, https://doi.org/10.1002/jcc.24015.
[34] H.J.C. Berendsen, J.P.M. Postma, W.F. Vangunsteren, A. Dinola, J.R. Haak, Molecular-dynamics with coupling to an external bath, J. Chem. Phys. 81 (1984) 3684–3690, https://doi.org/10.1063/1.448118.
[35] C.I. Bayly, P. Cieplak, W. Cornell, P.A. Kollman, A well-behaved electrostatic potential based method using charge restraints for deriving atomic charges: the RESP model, J. Phys. Chem. 97 (1993) 10269–10280, https://doi.org/10.1021/j100142a004.
[36] M.J. Frisch, G.W. Trucks, H.B. Schlegel, G.E. Scuseria, M.A. Robb, J.R. Cheeseman, G. Scalmani, V. Barone, B. Mennucci, G.A. Petersson, H. Nakatsuji, M. Caricato, X. Li, H.P. Hratchian, A.F. Izmaylov, J. Bloino, G. Zheng, J.L. Sonnenberg, Gaussian 09, Revision E.01, Gaussian, Inc., Wallingford, CT, 2009.
[37] M.A. Martí, A. Crespo, L. Capece, L. Boechi, D.E. Bikiel, D.A. Scherlis, D.A. Estrin, Dioxygen affinity in heme proteins investigated by computer simulation, J. Inorg. Biochem. 100 (2006) 761–770, https://doi.org/10.1016/j.jinorgbio.2005.12.009.
[38] D.E. Bikiel, L. Boechi, L. Capece, A. Crespo, P.M.D. Biase, S.D. Lella, M.C. G. Lebrero, M.A. Martí, A.D. Nadra, L.L. Perissinotti, D.A. Scherlis, D.A. Estrin, Modeling heme proteins using atomistic simulations, Phys. Chem. Chem. Phys. 8 (2006) 5611–5628, https://doi.org/10.1039/B611741B.
[39] L.L. Perissinotti, M.A. Martí, F. Doctorovich, F.J. Luque, D.A. Estrin, A microscopic study of the deoxyhemoglobin-catalyzed generation of nitric oxide from nitrite anion, Biochemistry. 47 (2008) 9793–9802, https://doi.org/10.1021/bi801104c.
[40] H.J. Nothnagel, N. Love, J.T.J. Lecomte, The role of the heme distal ligand in the post-translational modification of *Synechocystis* hemoglobin, J. Inorg. Biochem. 103 (2009) 107–116, https://doi.org/10.1016/j.jinorgbio.2008.09.009.
[41] D. Giordano, L. Boechi, A. Vergara, M.A. Martí, U. Samuni, D. Dantsker, L. Grassi, D.A. Estrin, J.M. Friedman, L. Mazzarella, G. di Prisco, C. Verde, The hemoglobins of the sub-Antarctic fish *Cottoperca gobio*, a phyletically basal species – oxygen-binding equilibria, kinetics and molecular dynamics, FEBS J. 276 (2009) 2266–2277, https://doi.org/10.1111/j.1742-4658.2009.06954.x.
[42] L. Capece, A. Lewis-Ballester, M.A. Martí, D.A. Estrin, S.-R. Yeh, Molecular basis for the substrate stereoselectivity in tryptophan dioxygenase, Biochemistry. 50 (2011) 10910–10918, https://doi.org/10.1021/bi201439m.
[43] F. Forti, L. Boechi, D. Bikiel, M.A. Martí, M. Nardini, M. Bolognesi, C. Viappiani, D. Estrin, F.J. Luque, Ligand migration in *Methanosarcina acetivorans* protoglobin: effects of ligand binding and dimeric assembly, J. Phys. Chem. B 115 (2011) 13771–13780, https://doi.org/10.1021/jp208562b.
[44] W. Humphrey, A. Dalke, K. Schulten, VMD: visual molecular dynamics, J. Mol. Graph. 14 (1996) 33–38, https://doi.org/10.1016/0263-7855(96)00018-5.
[45] A. Crespo, M.A. Martí, D.A. Estrin, A.E. Roitberg, Multiple-steering QM-MM calculation of the free energy profile in chorismate mutase, J. Am. Chem. Soc. 127 (2005) 6940–6941, https://doi.org/10.1021/ja0452830.
[46] A. Crespo, D.A. Scherlis, M.A. Martí, P. Ordejón, A.E. Roitberg, D.A. Estrin, A DFT-based QM-MM approach designed for the treatment of large molecular systems: application to chorismate mutase, J. Phys. Chem. B 107 (2003) 13728–13736, https://doi.org/10.1021/jp036236h.
[47] M.A. Martí, L. Capece, A. Crespo, F. Doctorovich, D.A. Estrin, Nitric oxide interaction with cytochrome *c*' and its relevance to guanylate cyclase. Why does the iron histidine bond break? J. Am. Chem. Soc. 127 (2005) 7721–7728, https://doi.org/10.1021/ja042870c.
[48] M.A. Martí, A. Crespo, S.E. Bari, F.A. Doctorovich, D.A. Estrin, QM-MM study of nitrite reduction by nitrite reductase of *Pseudomonas aeruginosa*, J. Phys. Chem. B 108 (2004) 18073–18080, https://doi.org/10.1021/jp048807r.
[49] A.D. Becke, Density-functional exchange-energy approximation with correct asymptotic behavior, Phys. Rev. A 38 (1988) 3098–3100, https://doi.org/10.1103/PhysRevA.38.3098.
[50] S. Chiodo, N. Russo, E. Sicilia, Newly developed basis sets for density functional calculations, J. Comput. Chem. 26 (2005) 175–184, https://doi.org/10.1002/jcc.20144.
[51] D.A. Case, V. Babin, J. Berryman, R.M. Betz, Q. Cai, D.S. Cerutti, T.E. Cheatham III, T.A. Darden, R.E. Duke, H. Gohlke, A.W. Goetz, S. Gusarov, N. Homeyer, P. Janowski, J. Kaus, I. Kolossváry, A. Kovalenko, T.S. Lee, S. LeGrand, T. Luchko, R. Luo, B. Madej, K.M. Merz, F. Paesani, D.R. Roe, A. Roitberg, C. Sagui, R. Salomon-Ferrer, G. Seabra, C.L. Simmerling, W. Smith, J. Swails, R.C. Walker, J. Wang, R.M. Wolf, X. Wu, P.A. Kollman, Amber 14, University of California, San Francisco, 2014. http://hdl.handle.net/10993/16614.
[52] M. Eichinger, P. Tavan, J. Hutter, M. Parrinello, A hybrid method for solutes in complex solvents: density functional theory combined with empirical force fields, J. Chem. Phys. 110 (1999) 10452–10467, https://doi.org/10.1063/1.479049.
[53] M.A. Martí, L. Capece, A. Bidon-Chanal, A. Crespo, V. Guallar, F.J. Luque, D. A. Estrin, Nitric oxide reactivity with globins as investigated through computer simulation, Methods Enzymol. 437 (2008) 477–498, https://doi.org/10.1016/S0076-6879(07)37024-9.
[54] A. Lewis-Ballester, D. Batabyal, T. Egawa, C. Lu, Y. Lin, M.A. Martí, L. Capece, D. A. Estrin, S.-R. Yeh, Evidence for a ferryl intermediate in a heme-based dioxygenase, Proc. Natl. Acad. Sci. U. S. A. 106 (2009) 17371–17376, https://doi.org/10.1073/pnas.0906655106.
[55] L. Capece, A. Lewis-Ballester, S.-R. Yeh, D.A. Estrin, M.A. Marti, Complete reaction mechanism of indoleamine 2,3-dioxygenase as revealed by QM/MM simulations, J. Phys. Chem. B 116 (2012) 1401–1413, https://doi.org/10.1021/jp2082825.
[56] B. Pinter, R. Al-Saadon, Z. Chen, W. Yang, Spin-state energetics of iron (II) porphyrin from the particle-particle random phase approximation, Eur. Phys. J. B. 91 (2018) 270, https://doi.org/10.1140/epjb/e2018-90169-6.
[57] D.A. Scherlis, D.A. Estrin, Structure and spin-state energetics of an iron porphyrin model: an assessment of theoretical methods, Int. J. Quantum Chem. 87 (2002) 158–166, https://doi.org/10.1002/qua.10043.
[58] I. Birukou, R.L. Schweers, J.S. Olson, Distal histidine stabilizes bound O_2 and acts as a gate for ligand entry in both subunits of adult human hemoglobin, J. Biol. Chem. 285 (2010) 8840–8854, https://doi.org/10.1074/jbc.M109.053934.
[59] F. Yang, G.N. Phillips Jr., Crystal structures of CO-, deoxy- and met-myoglobins at various pH values, J. Mol. Biol. 256 (1996) 762–774, https://doi.org/10.1006/jmbi.1996.0123.
[60] S.E.V. Phillips, D. Hall, M.F. Perutz, Structure of deoxyhaemoglobin Zürich (HisE7 (63β) — > Arg), J. Mol. Biol. 150 (1981) 137–141, https://doi.org/10.1016/0022-2836(81)90329-6.
[61] J. Qin, U. Pande, G.N.L. Mar, F. Ascoli, P. Ascenzi, F. Cutruzzolá, C. Travaglini-Allocatelli, M. Brunori, ^{1}H NMR study of the dynamics of the pH modulation of axial coordination in *Aplysia limacina* (Val(E7)) and sperm whale double mutant His(E7)–>Val,Thr(E10)–>Arg metmyoglobin, J. Biol. Chem. 268 (1993) 24012–24021.
[62] Y. Yamamoto, T. Suzuki, H. Hori, Dynamics and thermodynamics of acid-alkaline transitions in metmyoglobins lacking the usual distal histidine residue, BBA-Protein Struct. M. 1203 (1993) 267–275, https://doi.org/10.1016/0167-4838(93)90093-7.
[63] C. Travaglini-Allocatelli, F. Cutruzzola, A. Brancaccio, M. Brunori, J. Qin, G.N. La Mar, Structural and functional characterization of sperm whale myoglobin mutants: role of arginine (E10) in ligand stabilization, Biochemistry 32 (1993) 6041–6049, https://doi.org/10.1021/bi00074a015.
[64] T. Kuwada, T. Hasegawa, T. Takagi, I. Sato, F. Shishikura, pH-dependent structural changes in haemoglobin component V from the midge larva *Propsilocerus akamusi* (Orthocladiinae, Diptera), Acta Cryst. D. 66 (2010) 258–267, https://doi.org/10.1107/S0907444909055760.
[65] D.B. Nye, E.A. Johnson, M.H. Mai, J.T.J. Lecomte, Replacement of the heme axial lysine as a test of conformational adaptability in the truncated hemoglobin THB1, J. Inorg. Biochem. 201 (2019) 110824, https://doi.org/10.1016/j.jinorgbio.2019.110824.
[66] C.A. Wraight, Chance and design — Proton transfer in water, channels and bioenergetic proteins, Biochim. Biophys. Acta 1757 (2006) 886–912, https://doi.org/10.1016/j.bbabio.2006.06.017.
[67] J.P. Arcon, P. Rosi, A.A. Petruk, M.A. Martí, D.A. Estrin, Molecular mechanism of myoglobin autoxidation: insights from computer simulations, J. Phys. Chem. B 119 (2015) 1802–1813, https://doi.org/10.1021/jp5093948.
[68] W.J. Wallace, R.A. Houtchens, J.C. Maxwell, W.S. Caughey, Mechanism of autooxidation for hemoglobins and myoglobins. Promotion of superoxide production by protons and anions, J. Biol. Chem. 257 (1982) 4966–4977, https://doi.org/10.1016/S0021-9258(18)34620-9.
[69] R.E. Brantley, S.J. Smerdon, A.J. Wilkinson, E.W. Singleton, J.S. Olson, The mechanism of autooxidation of myoglobin, J. Biol. Chem. 268 (1993) 6995–7010, https://doi.org/10.1016/S0021-9258(18)53138-0.
[70] M.A. Martí, A. Bidon-Chanal, A. Crespo, S.-R. Yeh, V. Guallar, F.J. Luque, D. A. Estrin, Mechanism of product release in NO detoxification from *Mycobacterium tuberculosis* truncated hemoglobin N, J. Am. Chem. Soc. 130 (2008) 1688–1693, https://doi.org/10.1021/ja076853+.